Seasonal forcing in a host–macroparasite system

Taylor, Rachel A.; White, Andrew Ronald; Sherratt, Jonathan Adam

Published in:
Journal of Theoretical Biology

DOI:
10.1016/j.jtbi.2014.10.007

Publication date:
2015

Seasonal Forcing in a Host-Macroparasite System

Rachel A. Taylor*, Andrew White†, Jonathan A. Sherratt‡

Abstract

Seasonal forcing represents a pervasive source of environmental variability in natural systems. Whilst it is reasonably well understood in interacting populations and host-microparasite systems, it has not been studied in detail for host-macroparasite systems. In this paper we analyse the effect of seasonal forcing in a general host-macroparasite system with explicit inclusion of the parasite larval stage and seasonal forcing applied to the birth rate of the host. We emphasise the importance of the period of the limit cycles in the unforced system on the resulting dynamics in the forced system. In particular, when subject to seasonal forcing host-macroparasite systems are capable of multi-year cycles, multiple solution behaviour, quasi-periodicity and chaos. The host-macroparasite systems show a larger potential for multiple solution behaviour and a wider range of periodic solutions compared to similar interacting population and microparasite systems. By examining the system for parameters that represent red grouse and the macroparasite nematode *Trichostrongylus tenuis* we highlight how seasonality could be an important factor in explaining the wide range of seemingly uncorrelated cycle periods observed in grouse abundance in England and Scotland.

1 Introduction

Seasonal forcing is a ubiquitous force in nature affecting species through their life-history parameters, with an annual pulse of births in spring and summer seen as perhaps its most pervasive manifestation (Turchin, 2003). Seasonal forcing has been shown to be important in generating the cycles observed in many ecological and epidemiological systems. For example, by including seasonal forcing to represent changes in transmission during the school year, modelling results have been shown to be consistent with observations of measles case reports (Altizer et al., 2006; Earn et al., 2000; Finkenstadt and Grenfell, 2000). Numerous other examples exist in which seasonal forcing has been shown to be a driver of fluctuations: including outbreaks of influenza (Dushoff et al., 2004), plankton-fish dynamics (Doveri et al., 1993) and vole population cycles

*Corresponding address: rat3@hw.ac.uk, Department of Mathematics, Heriot-Watt University, Edinburgh, UK
†Department of Mathematics, Heriot-Watt University, Edinburgh, UK
‡Department of Mathematics, Heriot-Watt University, Edinburgh, UK

(Smith et al., 2008; Taylor et al., 2013b). Thus, within the field of interacting populations and host-microparasite systems, the importance of seasonal forcing is both well-established and well-studied (Altizer et al., 2006; Sherratt and Smith, 2008).

Seasonal forcing within host-macroparasite systems is less well identified and studied. In part, this may be because seasonality is associated with its ability to produce cyclic dynamics and these are less frequently reported in macroparasite compared to microparasite systems (Gulland, 1995; White et al., 1996). However, there are significant examples where macroparasites are thought to be influential in driving population cycles. Red grouse fluctuate irregularly across England and Scotland (Cattadori et al., 2005b; Haydon et al., 2002) and the role of nematode parasites, alongside territorial dynamics, in driving these cycles has been strongly argued (Dobson and Hudson, 1992; Hudson et al., 1998; Redpath et al., 2006). Soay sheep have population crashes every 3 to 4 years, which have been attributed to nematode parasites in combination with harsh winters and malnutrition (Coulson et al., 2001; Gulland and Fox, 1992; Gulland, 1992). There is considerable evidence to indicate that seasonal forcing alters many aspects of both these systems, such as the host birth rate, the maturation of parasite larvae in the environment, and arrested development of larvae within the host (Anderson, 2000), which could impact on the dynamics. However, no detailed analysis has been attempted to elucidate the effect of seasonal forcing alongside parasitism for these systems.

Theoretical studies of seasonal forcing in general host-macroparasite systems have been of two types. Roberts and Grenfell (1991, 1992) explored system specific model frameworks to understand the effect of a periodic pulse on the level of acquired host immunity and how environmental forcing on maturation of the nematode larvae affects the epidemiological dynamics of farmed ruminants. This work has been extended to consider wildlife systems, focussing on how host immunity and the relationship between host age and parasite intensity changes over one season within the host (Cattadori et al., 2005a; Cornell et al., 2008). These studies found that the host immune response was affected by both seasonal changes in larvae transmission and the month of host birth; therefore different host age – parasite intensity curves exist for different birth cohorts. General host-macroparasite models have examined the role of seasonality on population dynamics by representing annual reproduction as a step-function (White et al., 1996) and a pulse of births (White and Grenfell, 1997). When free-living stages are considered explicitly, seasonality can increase the period and amplitude of population cycles and there is evidence of multiple population attractors (White et al., 1996), although there has not been a detailed investigation of these findings. Therefore a detailed examination of the role of seasonality on host-macroparasite dynamics is lacking and could utilize the recent developments in

computational bifurcation theory and resonance-based analysis that have been applied to understand population cycles in microparasite and interacting systems (Bolzoni et al., 2008; Choisy et al., 2006; Greenman et al., 2004; Taylor et al., 2013a).

Experimental and theoretical studies highlight the need to explore seasonal effects in host-macroparasite systems. In this paper we propose to undertake a comprehensive analysis of the role of seasonality on host-macroparasite population dynamics that utilizes the new developments in the study of forced coupled systems (Taylor et al., 2013a). We will undertake this analysis in a system that explicitly represents free-living stages of the parasite, since White et al. (1996) indicated that seasonality could have a marked effect in such systems. This allows us to understand the wide range of outcomes occurring from seasonal forcing in general host-macroparasite systems. In particular, we will show the importance of the unforced dynamics on the seasonally forced system and the possibility of multiple solution behaviour, multi-year cycles and period-doubling to chaos. Furthermore, such model formulations without seasonal forcing have been parameterised to represent the red grouse - *Trichostrongylus tenuis* system (Dobson and Hudson, 1992) and therefore our results will provide important insight into the influence of seasonality on the population dynamics in a specific ecological system.

2 Methods

Macroparasites (helminths) differ from microparasites (viruses, bacteria, protozoa) in that they reproduce by releasing free-living infective stages, which mature in the environment or a secondary host before being transmitted to the definitive host. They usually have a relatively long life span and are persistent in the host with multiple re-infections being typical (Anderson and May, 1992). This added complexity in the life cycle of the macroparasite leads to the necessity of modelling the parasite burden within each host explicitly. A pattern seen across a wide range of different host and parasite species is that a minority of hosts within the population harbour the majority of parasites (Anderson and May, 1978; Wilson et al., 2002); regularly more than 80% of parasites are contained within 20% of the hosts (Anderson and May, 1992). Macroparasites can cause a reduction in breeding capabilities of the host, by modifying host behaviour or lowering the average brood size. Reduced survival is also possible indirectly, by making the host more susceptible to predation, and when hosts contain large numbers of parasites, this can become a direct cause of death (Anderson and May, 1978, 1992; Gulland, 1995; Hudson et al., 1992).

Numerous models have been used to represent host-macroparasite systems, with different frameworks for including aggregation, the effect of immunity, arrested development and larval dynamics (Anderson and May, 1978; Diekmann and Kretzschmar, 1991; May and Anderson,

1978; Rosà and Pugliese, 2002; White et al., 1996; White and Grenfell, 1997). In this paper we build on previous studies by using a general model formulation which includes exponential growth of the host, models the larval stage explicitly, and the aggregation of parasite spread throughout hosts is represented by the commonly used negative binomial distribution (Anderson and May, 1978; Rosà and Pugliese, 2002; White and Grenfell, 1997). This produces the following system of equations:

$$\begin{aligned}\frac{dH}{d\tau} &= (a^* - b)H - (\alpha + \delta^*)P \\ \frac{dP}{d\tau} &= \beta^* LH - (\mu^* + b + \alpha)P - \alpha\frac{P^2}{H}\left(\frac{k+1}{k}\right) \\ \frac{dL}{d\tau} &= \lambda P - \gamma^* L - \beta^* LH.\end{aligned} \tag{2.1}$$

A derivation of this model is provided in Appendix A. $H(\tau)$ is the number of host species at time τ, $P(\tau)$ is the total number of adult parasites contained within all of the hosts at time τ and $L(\tau)$ is the number of free-living larval stage parasites. The host species undergoes exponential birth and death, with rates a^* and b respectively, as well as death, αP, and reduced fecundity, $\delta^* P$, caused by the parasite. The term $\beta^* LH$ denotes the rate of transmission of larvae to hosts leading to adult parasites. Parasites are lost due to natural mortality with rate μ^*, natural death of the host (rate b) and parasite induced death of the host. However, host death due to parasitism requires knowledge of expected number of parasites within each host, and we assume a negative binomial distribution for the parasites with aggregation parameter k (which leads to the form of (2.1)). Finally, the larvae are produced by adult parasites laying eggs at rate λ and die at rate γ^*.

We non-dimensionalise this model, with the scalings, $h = \frac{\beta^* H}{b}$, $p = \frac{\alpha\beta^* P}{b^2}$, $l = \frac{\alpha\beta^* L}{\lambda b}$ and $t = b\tau$. The new parameters are $a = \frac{a^*}{b}$, $\delta = \frac{\delta^*}{\alpha}$, $\beta = \frac{\lambda}{b}$, $\mu = \frac{\mu^* + \alpha}{b}$ and $\gamma = \frac{\gamma^*}{b}$. This produces the following model:

$$\begin{aligned}\frac{dh}{dt} &= (a-1)h - (1+\delta)p \\ \frac{dp}{dt} &= \beta lh - (\mu+1)p - \frac{p^2}{h}\left(\frac{k+1}{k}\right) \\ \frac{dl}{dt} &= p - \gamma l - lh.\end{aligned} \tag{2.2}$$

Our work is not specifically focussed on red grouse; rather we use this example to elucidate our results for the effects of introducing a seasonally forced birth rate into host-macroparasite systems. Red grouse (*Lagopus lagopus scoticus*) are a common case study for macroparasites due to the relative simplicity of the parasite dynamics, the interesting cyclic dynamics seen across England and Scotland and the availability of data from hunting records. The adult nematode *Trichostrongylus tenuis* lives in the caeca of the grouse, passing eggs out of the host through

the caecal faeces. The larvae mature in the environment (if conditions are suitable) and then migrate to the tips of heather. The grouse ingest these larvae by eating the heather, their main food plant (Anderson, 2000; Hudson et al., 1992). Experimental studies have shown that the nematode *Trichostrongylus tenuis* reduces reproduction in red grouse populations through lower clutch sizes, egg mortality and chick loss (Hudson et al., 1992), thus Dobson and Hudson (1992) emphasised the reduced fecundity term, δ. In Dobson and Hudson (1992) the above model (2.1) is parameterised for the red grouse system as shown and also when there is the addition of a logistic growth term. For consistency with other studies of host-macroparasite systems (White et al., 1996; White and Grenfell, 1997), we use the exponential growth model and the parameter values provided by Dobson and Hudson (1992), which after rescaling become: $a = 1.7$, $\beta = 10/1.05$, $\mu = 1.0003/1.05$, $k = 1$ and $\gamma = 10/1.05$. These rates are defined per year. Dobson and Hudson (1992) let $\delta = 1.667$, which combined with the other parameter values leads to diverging cycles driving the hosts and parasites to extinction. This can be counteracted by adding host regulation through logistic growth or by varying the value of δ and analysing the effect of this on the dynamics, which is shown throughout this study. The influence of seasonal forcing in the model with host regulation included would be a natural area for future study.

We introduce seasonal forcing into the birth rate of the host, using a sinusoidal form, a common method for representing seasonal changes (Choisy et al., 2006; Dietz, 1976; Rinaldi et al., 1993). The birth rate becomes

$$a(t) = a(1 + \epsilon \sin(2\pi t)) \tag{2.3}$$

where a is the mean value of the forced birth rate (the same value as in the unforced case, $a = 1.7$) and ϵ is the amplitude of the forcing.

2.1 Unforced dynamics

In order to understand the effect of seasonal forcing, we first need to consider the unforced dynamics. The system (2.2) undergoes a Hopf bifurcation when δ is varied, with a stable equilibrium for $\delta < 0.78$ and stable limit cycles for δ above this value. Explicit inclusion of the larval stage is somewhat akin to the addition of a time delay and this is fundamental in causing the cycles. In Figure 1 the period and amplitude of these limit cycles are plotted as a function of δ.

As shown in Figure 1, the period of the limit cycles starts at 5.9 years and increases rapidly as δ increases. Previous studies (Greenman et al., 2004; Rinaldi et al., 1993; Taylor et al., 2013a) have shown how yearly forcing can resonate with the unforced period at integer values to produce multi-year cycles of that integer period or multiples thereof. Thus, we do not expect

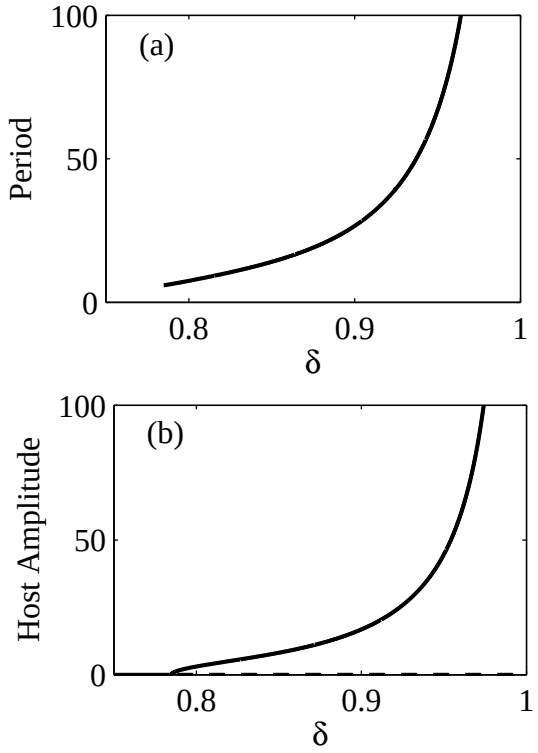

Figure 1: In (a) the period of the limit cycles is plotted as δ is varied. In (b) the amplitudes of the steady state and the limit cycles are plotted as δ is varied. Stability and instability are indicated by the solid and dashed lines respectively. All other parameter values are kept constant with the following values: $a = 1.7$, $\beta = \gamma = 10/1.05$, $\mu = 1.0003/1.05$ and $k = 1$.

to be able to find multi-year solutions which have period less than 6 (since that is the smallest integer period that can be exhibited in the model for our parameter choice). The amplitude plot in Figure 1(b) shows the amplitude of the limit cycles also increasing rapidly as δ increases (and explains why divergent cycles leading to extinction occur for $\delta = 1.667$ in Dobson and Hudson (1992)).

2.2 Bifurcation Method

We will investigate the effects of seasonal forcing in this example by varying both δ and ϵ and show the multi-year dynamics and multiple solution behaviour that occur using a two-dimensional bifurcation diagram. We will then move on to a more general framework to understand seasonal forcing within host-macroparasite systems in greater detail. We begin with a brief overview of the necessary bifurcation theory; for more information please see references Kuznetsov (1995); Taylor et al. (2013a). There are three main bifurcation curves namely, period-doubling bifurcation curves, fold bifurcation curves and Neimark-Sacker bifurcation curves. The

standard procedure for locating bifurcations uses the Poincaré (or stroboscopic) map that transforms the continuous system into a discrete one by sampling the solution once in each forcing period; once per year in our case. Note that the stable/unstable annual cycles become stable/unstable fixed points of the Poincaré map. Discrete bifurcation theory reveals that this fixed point is unstable if one of the eigenvalues of its linearisation has modulus larger than 1. Changes in stability are of three possible types. If the eigenvalue is equal to -1, it is a period-doubling (flip) bifurcation; if the eigenvalue is equal to $+1$ it is a fold (saddle-node, tangent) bifurcation; and if there is a pair of complex conjugate eigenvalues with modulus 1, it is a Neimark-Sacker (torus) bifurcation.

At a period-doubling bifurcation curve, which we denote by PDk, a stable cycle of period k loses stability and a stable cycle of period $2k$ arises. On one side of a fold bifurcation curve denoted by FDk there is no solution but on the other side there are both stable and unstable solution branches of a cycle of period k, which meet at a fold at the bifurcation point. A Neimark-Sacker bifurcation is often described as a discrete version of a Hopf bifurcation because for a standard supercritical bifurcation, the fixed point on the Poincaré section becomes unstable and a stable closed invariant curve arises around the point. Typically, each iteration of the Poincaré map brings the solution back to a different point on the closed invariant curve. Therefore, in the continuous setting when crossing a Neimark-Sacker bifurcation curve, denoted by NSk, a cycle of period k loses stability and a quasi-periodic solution arises. That is, the solution may superficially appear periodic but in fact it has no finite period. Thus, there are different Neimark-Sacker bifurcation curves and separate regions of quasi-periodicity related to each of the different periodic solutions.

We use AUTO bifurcation software (Doedel, 1981) to produce the bifurcation diagrams and Matlab (`ode15s`) to produce numerical simulations. The simulations were run for 7000 years with initial conditions randomly chosen; arbitrarily we use a uniform distribution between 0 and 1. We then tested whether they had an exact period of between 1 and 16 years. If the simulations did not have an exact period within this range, they were labelled as quasi-periodic. Note that we also log-transformed the equations to speed up computational time as the solutions spend a large proportion of each cycle very close to zero and it takes a long time for the transient dynamics to die out. Log-transforming the equations significantly improves both computational time in Matlab and accuracy in AUTO. However, we reverse this log-transformation before presenting results.

3 Results

We consider first the host-macroparasite system with the red grouse parameters. This highlights key properties of seasonal forcing in host-macroparasites systems, such as a wide range of multi-year cycles of different periods, multiple solution behaviour and the possibility for increases in the amplitude of seasonal forcing alone to significantly change the dynamics. We then vary the model parameters, which has the effect of changing the unforced dynamics of the system and allows us to explore the effect of seasonal forcing on the host-macroparasite dynamics more generally.

3.1 The red grouse dynamics

In Figure 2, a two-dimensional bifurcation diagram is plotted for parameters representing the red grouse system showing the fold bifurcation curves and the Neimark-Sacker bifurcation curve. The Neimark-Sacker bifurcation curve (NS1) hits the $\epsilon = 0$ axis where the unforced system has a Hopf bifurcation. Below this curve there are stable yearly cycles - the effect of annual forcing on a stable equilibrium. Above the Neimark-Sacker bifurcation quasi-periodicity exists, caused by the annual forcing on the stable limit cycles. The Neimark-Sacker curve is almost horizontal, indicating that the unforced dynamics are a good predictor, in this case, of the split between yearly cycles and quasi-periodic dynamics. There are also regions of periodicity due to the resonance between the annual forcing and limit cycles with integer period, leading to the fold bifurcation curves. These curves originate from the $\epsilon = 0$ axis and diverge as ϵ increases with periodic behaviour possible within the fold boundaries. Note, however, that the curves indicate the existence of multi-year cycles but not their stability, which we will discuss later. The fold curves start at period 6 (FD6) which is the first integer greater than the lowest possible period in the unforced system (which is 5.9). The fold regions get larger as the period increases from period 6 to period 11 (FD6 is very narrow and FD11 is significantly wider). The fold regions decrease in size for regions greater than period 11 (not shown in Figure 2 but see Figure 5). No period-doubling of the yearly cycle occurs thus we do not find solutions with periods between 2-5 years inclusive.

The fold curves hit the axis at the value of δ at which the unforced limit cycles have the corresponding period, and the regions widen as ϵ increases from 0. The rapid increase of the unforced period with δ, as seen in Figure 1, leads to an overlap of the fold curves and indicates that there is potential for multiple solution behaviour. Moreover, some of the fold curves extend below the Neimark-Sacker bifurcation curve for larger values of ϵ. Thus, increasing the amplitude of seasonal forcing from 0 to 1 can change the system from a stable equilibrium to a yearly cycle

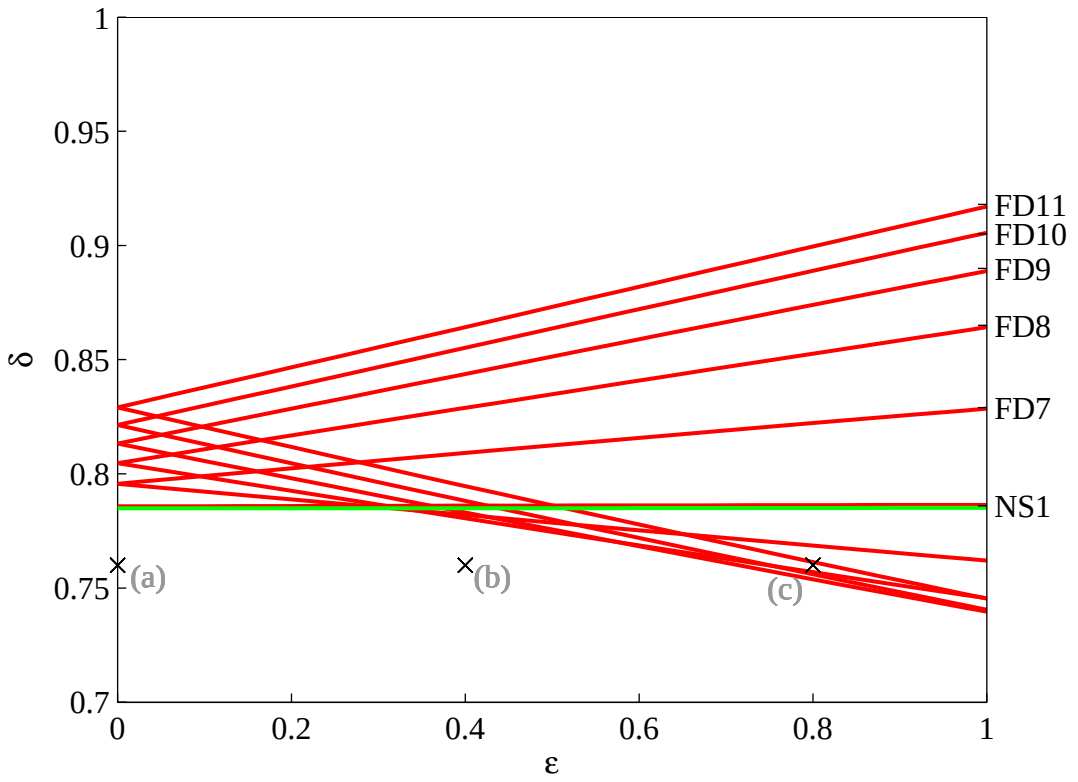

Figure 2: A two-dimensional bifurcation diagram in δ and ϵ. The Neimark-Sacker bifurcation curve is green, the fold curves are red. The FD6 curve lies almost on top of the NS1 curve. More fold curves exist with period higher than 11 but these are omitted to avoid over-complication. There is no period-doubling bifurcation. Only existence and not stability of the multi-year solutions is shown, outlined by the fold curves. The points labelled (a), (b) and (c) refer to the corresponding simulations in Figure 3. All other parameters values are kept constant with the following values: $a = 1.7$, $\beta = \gamma = 10/1.05$, $\mu = 1.0003/1.05$ and $k = 1$. (Colour online; Neimark-Sacker curve is dotted, fold curves are solid in print.)

to multi-year cycles, with no change in any other parameter (Figure 3). The multi-year cycles also have a significant increase in amplitude in comparison to the yearly cycle. Therefore, the inclusion of seasonal forcing can have a dramatic effect on the dynamics of the host and parasite for parameters corresponding to the red grouse system.

3.2 General Host-Macroparasite Dynamics

We wish to investigate further the effect of the unforced dynamics on the resulting multi-year cycles when forcing is introduced into the system. When the red grouse parameters are used, the model does not exhibit any multi-year cycles with period less than 6 (and the 6 year cycles

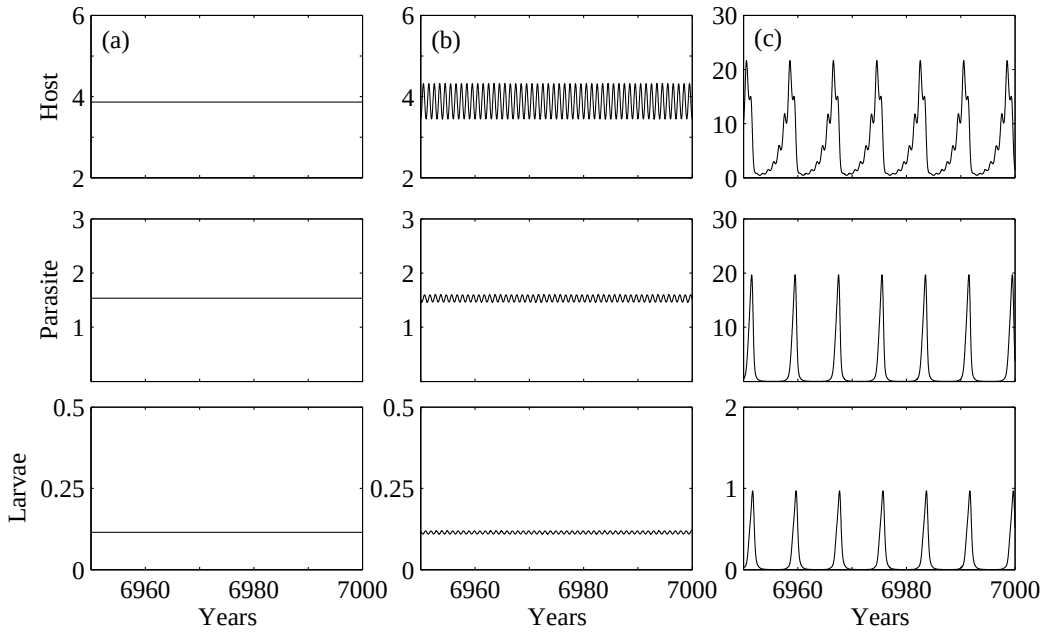

Figure 3: Simulations showing the effect of increasing the amplitude of forcing while all other parameters are kept constant. (a) $\epsilon = 0$; a stable equilibrium. (b) $\epsilon = 0.4$; a stable yearly cycle. (c) $\epsilon = 0.8$; a stable 8 year cycle (corresponding to the points labelled in Figure 2). The initial conditions are the same for all three simulations. $\delta = 0.76$ and all other details are as in Figure 2.

only for a very narrow range of δ-values). In comparison, interacting population and epidemiological systems frequently exhibit cycles with periods of 3-4 years (Earn et al., 2000; Korpimaki and Krebs, 1996). Are these higher period cycles observed purely because of the parameter values that are relevant for red grouse dynamics, or are they representative of our general host-macroparasite system?

To answer this question we consider the unforced dynamics in more detail and investigate the period at the Hopf bifurcation. As mentioned previously, the forcing only resonates with integer periods expressed in the unforced limit cycles. Thus, we investigated whether it is possible to reduce the initial period arising at the Hopf bifurcation so that the system will be able to resonate with lower period limit cycles. We varied the parameters in pairs, in order to stay on the Hopf bifurcation, and calculated the initial period at the Hopf bifurcation. We found that the host birth rate parameter a was the key driver of the period in the unforced system (regardless of the other parameter that was varied concurrently).

In Figure 4, we show how changing a affects the period at the Hopf bifurcation, and the corresponding changes in δ that are required in order to stay on the Hopf bifurcation. For $a < 1$ only the trivial steady state exists (where the host and parasite are absent). As a increases from

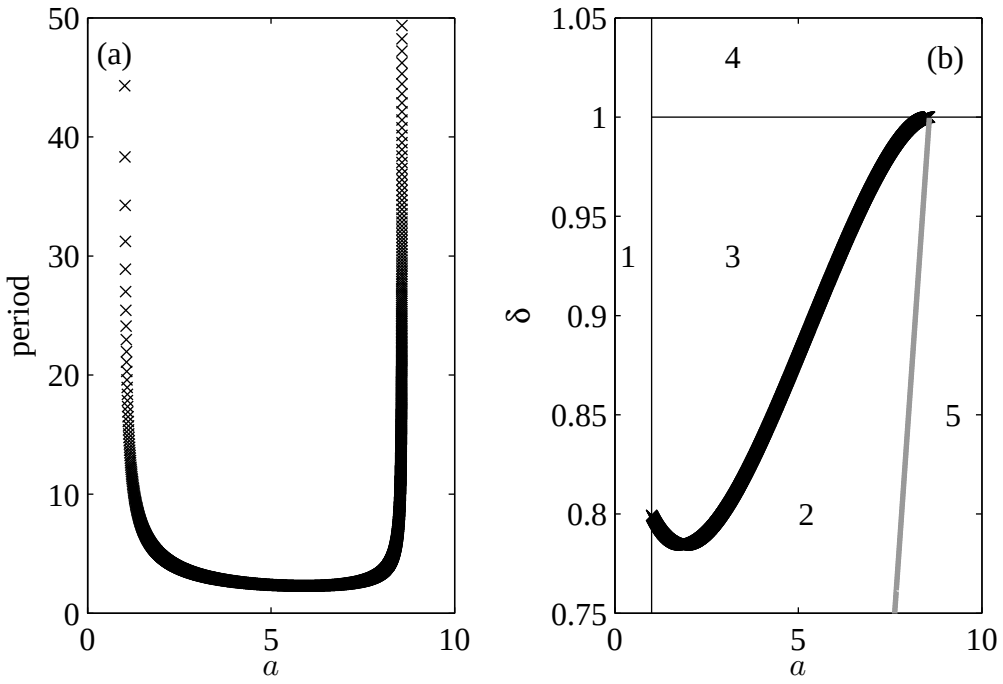

Figure 4: The Hopf bifurcation in the unforced system in more detail. In (a) the period at the Hopf bifurcation of the unforced system is plotted as a (and implicitly also δ) is varied. (b) The bifurcation diagram of the unforced system in a and δ. The thick black line is the Hopf bifurcation while the thick grey line indicates where the equilibrium is replaced by exponential growth. Dynamics by region: 1 - trivial equilibrium; 2 - stable equilibrium; 3 - stable limit cycles; 4 - diverging cycles driving host and parasite to extinction; 5 - exponential growth. All other details are as in Figure 1.

1 the period of the unforced system decreases with a minimum period of 2.3 years for $a = 5.9$. As a increases further the period increases and there is a rapid increase in period for $a > 8$ as δ approaches 1. For $\delta > 1$, there are diverging cycles that drive the host and parasite to extinction (Dobson and Hudson, 1992). For larger a the steady state increases in value because there is no host self-regulation in (2.2). The host and parasite populations experience exponential growth for parameter values in region 5 in Figure 4 as the parasites are unable to regulate the host population. Importantly, this shows that there is potential for lower period cycles in this model system. To understand how seasonal forcing interacts with the underlying period of the unforced system, we produce bifurcation diagrams in δ and ϵ for different values of a (Figure 5).

In Figure 5 the fold regions (red lines) for the different periods are plotted separately for each value of a. For lower values of a there are empty plots in the upper region of Figure 5 since here the cycle period is less than the initial period of the unforced dynamics (Figure 4).

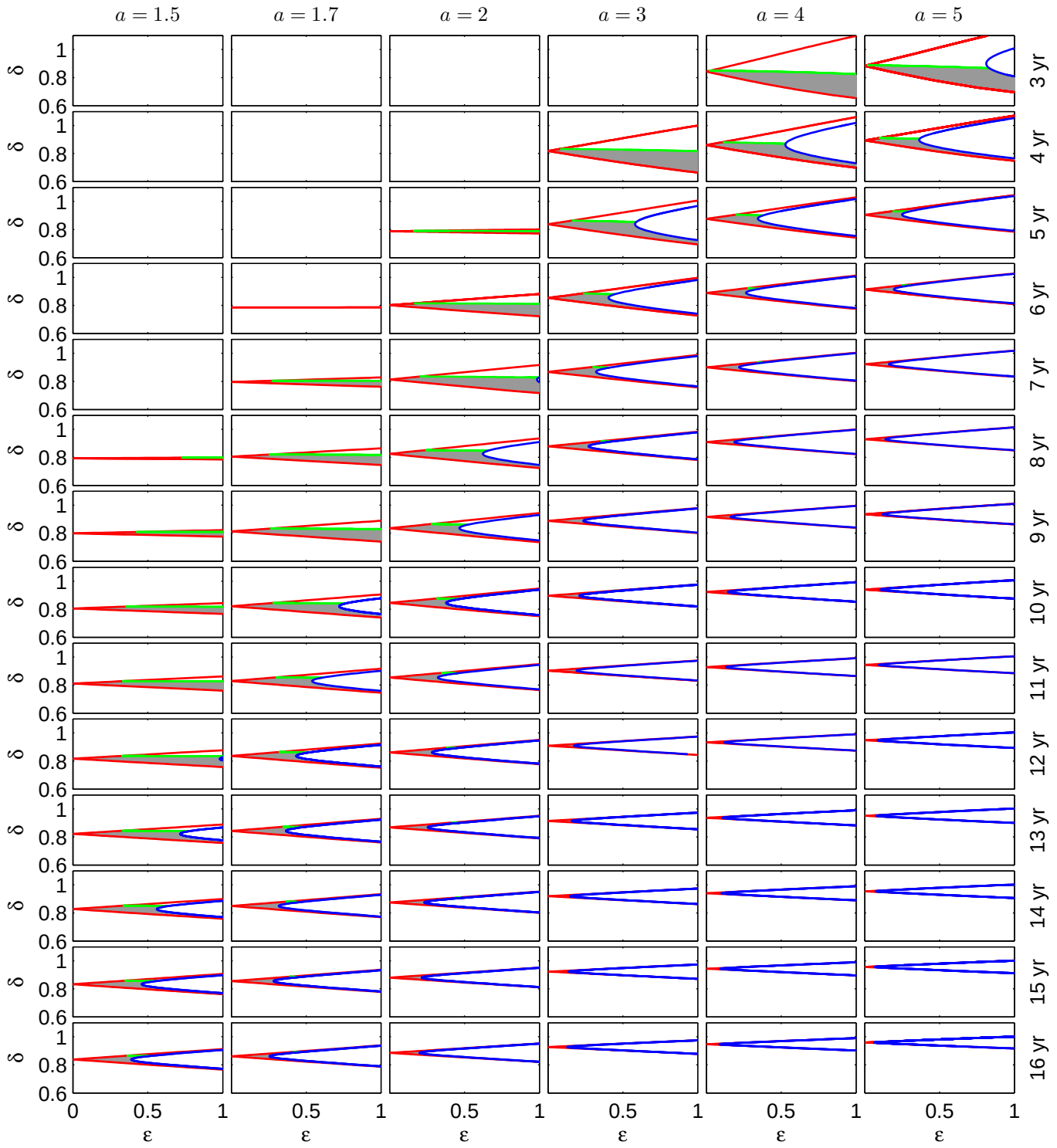

Figure 5: Bifurcation diagrams in δ and ϵ for different values of a. Each fold curve, outlining the different periodic regions, is plotted on a separate graph. The shaded regions indicate where each of the multi-year cycles are stable. Fold curves are red, period-doubling curves are blue and Neimark-Sacker bifurcation curves are green. Only those curves relevant to each particular multi-year cycle are plotted within each figure. For each value of a there is also a Neimark-Sacker bifurcation curve (NS1) indicating loss of stability of the yearly cycles but these aren't included. The 15 and 16 year fold curves for $a = 5$ stop before $\epsilon = 1$ due to continuation problems in AUTO (although not shown due to overlap of the period-doubling curves). All other details as in Figure 2. (Colour online; fold curves are thick black lines, period-doubling curves are thin

The fold regions are small if the period is close to the initial period. For example, suppose that the initial period at the Hopf bifurcation is either 5.2 or 5.9. The lowest possible period for multi-year cycles will be 6 years in both cases, but the 6 year fold region will be much smaller for the latter case. The fold regions start to decrease in size once the period is much larger than the initial period expressed in the unforced system. In general, there is a pattern of the largest fold regions occurring across a diagonal from top-right to bottom-left in Figure 5.

There is a significant difference between existence and stability of multi-year cycles in terms of the resulting dynamics of the system, and thus it is important to consider the region of stability of the multi-year cycles within each of the fold curves (i.e. the shaded regions in Figure 5). The presence of Neimark-Sacker bifurcation curves and period-doubling curves inside the fold curves leads to loss of stability of the multi-year cycles. For example, if we focus on the 3 year fold region for $a = 5$ (i.e. the top right plot in Figure 5), the 3 year cycles are stable in the shaded region, but crossing the Neimark-Sacker bifurcation curve for larger δ results in quasi-periodicity while crossing the period-doubling curve through increasing ϵ produces stable 6 year cycles. The size of the regions of stability follows a similar pattern to the fold regions: it decreases as the period increases for each value of a, mostly due to the period-doubling region inside the fold curves increasing in size. Notably, many of the fold curves contain only very small regions of stability, especially for the higher period cycles.

To investigate the potential for multiple solutions we superimpose the stable regions of the different multi-year solutions in Figure 5 for each value of a (Figure 6). The yearly Neimark-Sacker bifurcation curve (NS1) is shown but the fold, period-doubling and Neimark-Sacker curves for each of the multi-year cycles are omitted for clarity. There is considerable overlap of different stable multi-year regions implying that multiple solutions are possible for a fixed set of parameters. Figure 6 highlights the large effect that varying a has on the stability of multi-year cycles. This is further emphasised by noting that the stability regions shown in Figure 6(a) predominantly correspond to 10-14 year cycles whereas those in (f) have periods of 3-5 years, as seen in Figure 5.

To examine the likelihood of multiple solutions we ran simulations of our model system for four different parameter sets (indicated by the crosses in Figure 6) for 200 sets of initial conditions selected at random. Figure 7 indicates that multiple solution behaviour was observed. Both of the points which lie above the Neimark-Sacker bifurcation curves in Figure 6 (Figure 7(a),(c)) exhibit quasi-periodic dynamics while the two points below the curves (Figure 7(b),(d)) show yearly cycles as well as the multi-year cycles. Figure 7 also shows typical host population solutions for the four parameter sets, indicating that a range of annual, multi-year and quasi-

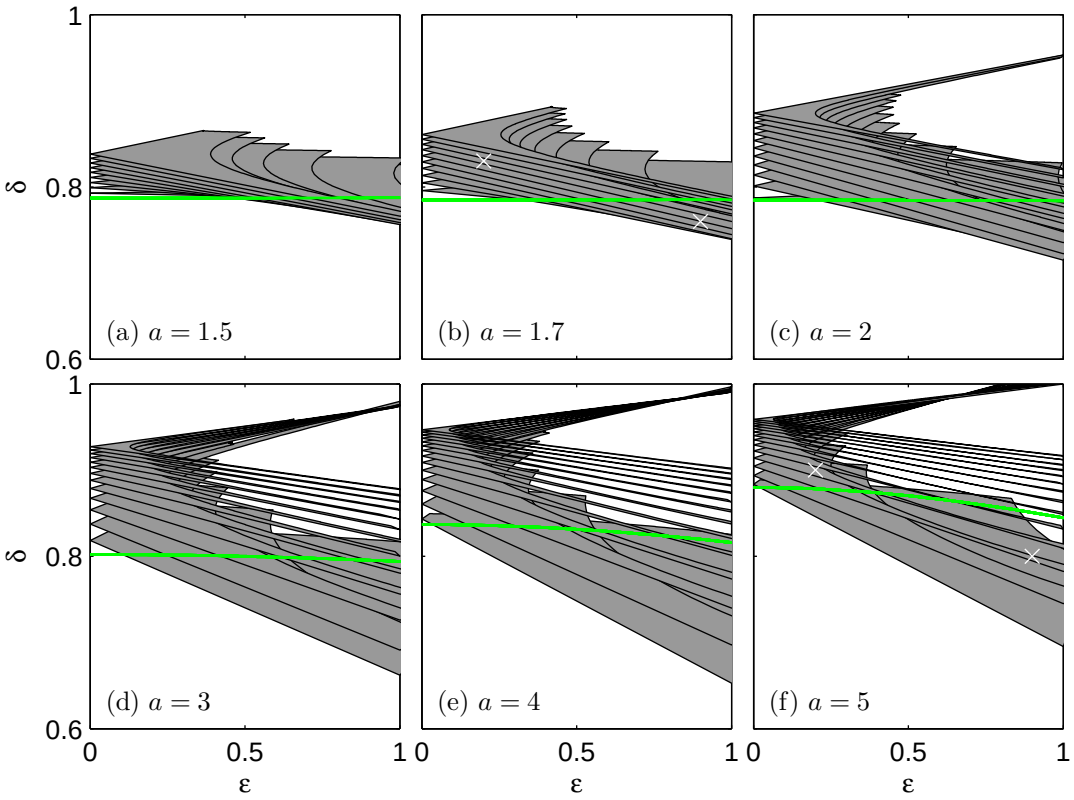

Figure 6: Two-dimensional bifurcation diagrams in δ and ϵ for each value of a showing only the stability regions (shaded) of the multi-year solutions. The Neimark-Sacker bifurcation curves (green online; grey dotted lines in print) indicate the change in stability of the yearly cycle, with yearly cycles stable below the line. The four crosses in (b) and (f) indicate the points that we used for testing multiple solution behaviour, as shown in Figure 7. All other details are the same as in Figure 2.

periodic behaviour can be exhibited. A wide range of amplitude is seen across the 12 simulations. This varies with cycle period, and with the values of ϵ, δ and a. For the case $a = 5$, it would be expected that there would mainly be low period cycles due to their larger regions of stability but there are some 16 year cycles. These 16 year cycles have peaks every 4 years, which suggests that they have arisen due to period-doubling (we examine this below). In comparison, a 16 year cycle that has arisen through the 16 year fold curve would usually have only one peak in the 16 year period.

In this more general framework of the host-macroparasite model we have shown that changing a has an important impact on the periodic solutions possible, with a greater likelihood of lower period multi-year cycles for the higher values of a tested. The overlap of stable regions for these multi-year cycles has been highlighted, and we have confirmed that multiple solution behaviour is possible, involving a wide range of cycle periods and amplitudes. We now move on to some

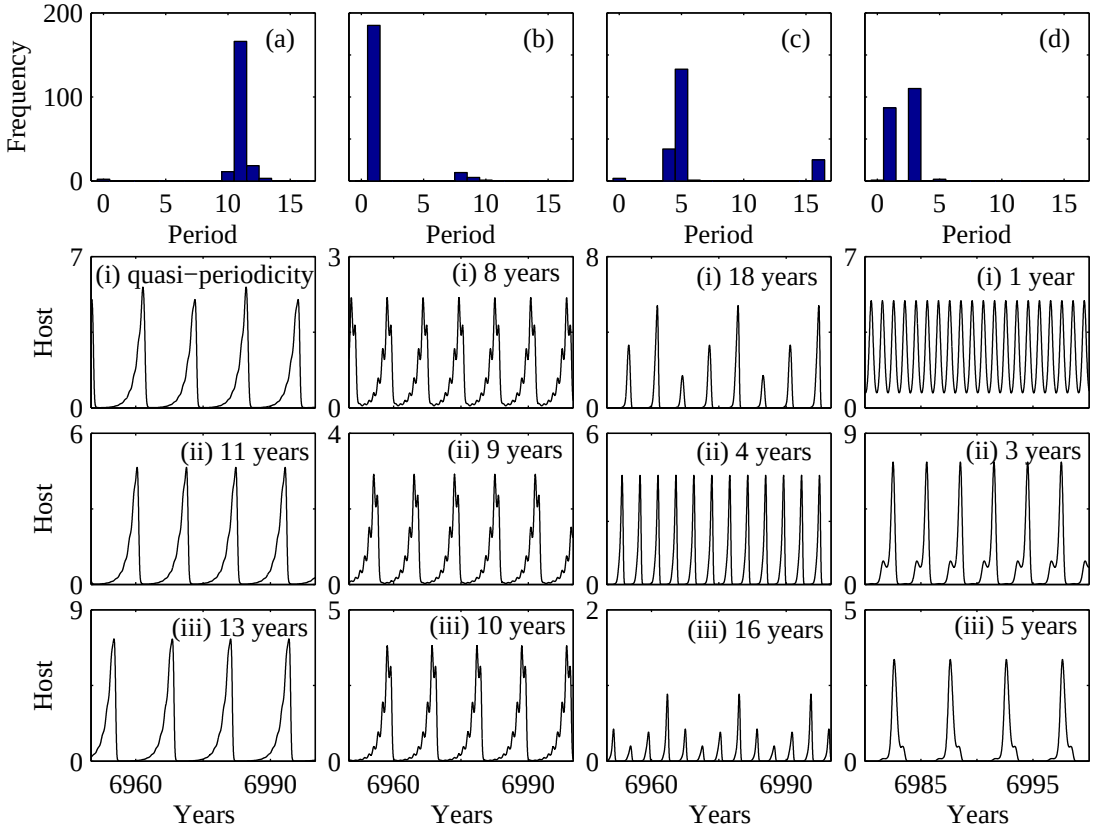

Figure 7: Investigating the potential for multiple solution behaviour. In (a) – (d) histograms show the results of 200 simulations for 4 different points (indicated on Figure 6). (a) $a = 1.7$, $\epsilon = 0.2$ and $\delta = 0.83$; (b) $a = 1.7$, $\epsilon = 0.9$ and $\delta = 0.76$; (c) $a = 5$, $\epsilon = 0.2$ and $\delta = 0.9$; and (d) $a = 5$, $\epsilon = 0.9$ and $\delta = 0.8$. Quasi-periodicity is represented by period 0 years. Three simulations of host populations are plotted for each histogram (in the same column) showing that different multi-year cycles are possible for that point. The period of the multi-year cycles are as shown. In (c)(i) the solution was calculated to be quasi-periodic but is actually an 18 year cycle (since we only test the simulations for periodicity of 16 years or lower). The simulations are not to scale; specifically (c)(i) $\times 10^5$, (c)(ii) $\times 10^3$, (c)(iii) $\times 10^4$, (d)(ii) $\times 10^2$, (d)(iii) $\times 10^4$ and the rest of the simulations are all $\times 10$. All other details are the same as in Figure 2.

of the more complicated aspects of these bifurcation diagrams for different values of a, such as the period-doubling bifurcations in Figure 5 and the overall effect of increasing the forcing amplitude ϵ.

3.3 Period-Doubling and Chaos

One aspect of Figure 5 which requires further attention is period-doubling inside the fold loci. Nearly all of the fold regions in Figure 5 contain period-doubling curves which indicate not

only the loss of stability of the cycles generated at the folds but also the generation of stable higher period cycles. Trying to show all this information on one plot, such as Figure 5, is rather complicated and thus we highlight one case (the 4 year cycles for $a = 4$) to show the full range of dynamics that can occur due to period-doubling (Figure 8).

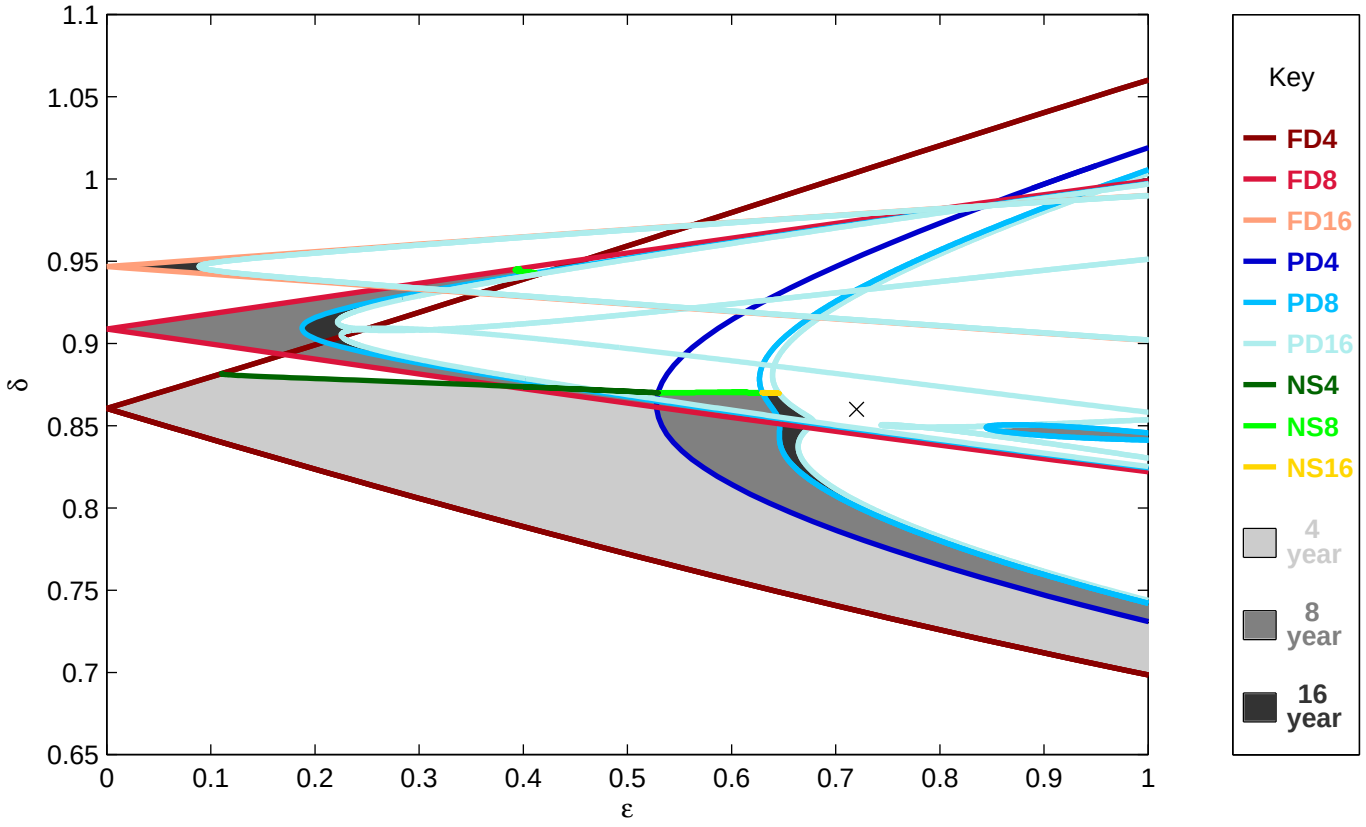

Figure 8: A bifurcation diagram in δ and ϵ showing only the 4, 8 and 16 year fold regions with their subsequent period-doubling bifurcations for the case $a = 4$. Both type and period of each curve is represented by the different colours. Stability of the different periodic solutions is shown by the shaded regions as indicated. The cross at $\epsilon = 0.72$, $\delta = 0.86$ corresponds to the simulation in Figure 9. All other details are as in Figure 2.

In Figure 8 there are three fold regions plotted, the largest being the 4 year fold region (FD4) in which the 4 year cycles lose stability as ϵ increases through a period-doubling bifurcation (PD4) leading to stable 8 year cycles. These 8 year cycles also undergo period-doubling (PD8) leading to stable 16 year cycles. Also shown is the 8 year fold region (FD8), in which the 8 year cycles lose stability through a period-doubling bifurcation (PD8) leading to stable 16 year cycles. And lastly, there is the 16 year fold region (FD16) which also indicates a region of stable 16 year cycles. All 3 of these stable 16 year regions lose stability through more period-doubling bifurcations (PD16). Moreover, period-halving occurs for large ϵ in the 4 year fold

region, leading to more regions of stable 8 and 16 year cycles (although the additional 16 year stable region is very small and not visible at this scale). This highlights that there are several routes that can lead to 16 year population cycles. It is interesting to note that the region of stability for the 16 year cycles resulting from two successive period-doublings of the 4 year cycles is larger than that for the 16 year fold curve, so that these period-doubling bifurcations are of key importance in providing information on the stable dynamics of the system. Also, the form of the period 16 cycles resulting from period-doubling and from the 16 year fold curve are very different, with only one peak every 16 years for the fold curve compared to a peak every 4 years for the period-doubled solution. There is also a significant difference in amplitude, which is much larger for the fold curve solution (this has been seen through extensive simulation; results not shown).

Figure 8 raises the possibility of chaos in this system through a period-doubling cascade. Within the 4 year fold curve there is a region after the 16 year cycles have lost stability before the period-halving begins, in which there is the suggestion of period-doubling to chaos. Simulation results have shown solutions which appear chaotic (Figure 9), although we have not tested this in detail.

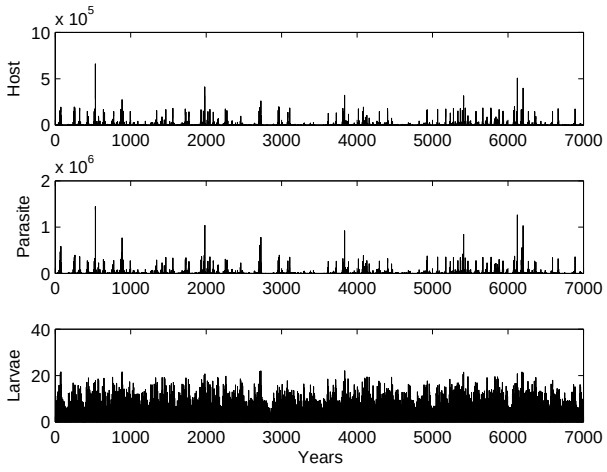

Figure 9: A simulation of an apparently chaotic solution. The fast Fourier transform method indicates a period of 70 years. Parameter values are $a = 4$, $\delta = 0.86$ and $\epsilon = 0.72$, indicated by a cross in Figure 8. All other details as in Figure 2.

Figure 8 is useful for exhibiting the complexities of the host-macroparasite model with seasonal forcing, especially when it is remembered that there are many other multi-year fold curves omitted from this figure, all with period-doubling regions which might lead to chaos. One common factor of all the multi-year cycles, as seen in Figures 5, 6 and 8 is that they lose stability as ϵ increases. Thus, an increase in seasonal forcing, with no changes in any other parameters, can

change the dynamics dramatically from multi-year limit cycles, to multi-year cycles of potentially different period due to the multiple solution behaviour and period-doubling, to quasi-periodicity and chaos. This again highlights the substantial impact of increasing the strength of the seasonal forcing on the dynamics.

The overlap of stable multi-year regions and the abundance of multiple solution behaviour indicate that the system may be sensitive to small perturbations in parameters or to noise. In Figure 10, a simulation shows the effect of a perturbation in the host population abundance (but no change of any parameters), which leads to a change in cycle period and amplitude. A similar perturbation in the corresponding unforced case would always settle back to the stable equilibrium as there are no multiple solutions. Overall, the host-macroparasite model when

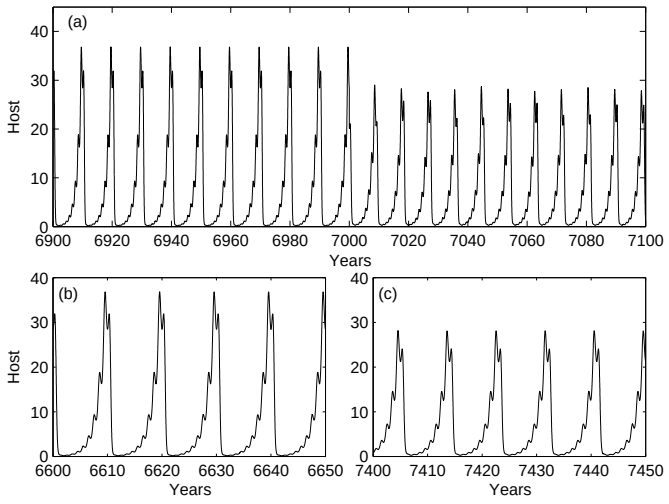

Figure 10: A simulation showing the effect of perturbations. A 10 year cycle is perturbed at 7000 years by changing the host population by 10%. It switches to a 9 year cycle. The transition in shown in (a) and the 10 and 9 year cycles are shown in more detail in (b) and (c) respectively for the host population. Parameter values are $a = 1.7$, $\delta = 0.77$, $\epsilon = 0.8$ and all other details are as in Figure 2.

subject to seasonal forcing is a complicated system with a wide range of possible dynamics depending on parameter values, the amplitude of the seasonal forcing and the initial conditions.

3.4 Results Summary

We have considered a general host-macroparasite model with reduced fecundity and explicit inclusion of a larval stage and explored the effects of introducing seasonal forcing through the host birth rate. When seasonal forcing is introduced into this host-macroparasite model it leads to stability of multi-year cycles, multiple stable solutions, period-doubling to higher period

cycles, quasi-periodicity and apparently chaotic behaviour. We studied this for different values of the host birth rate, parameter a in (2.2), as this leads to changes in the initial period of the unforced system at the Hopf bifurcation. For all values of a shown the unforced period of the limit cycles increases rapidly from the initial period at the Hopf bifurcation, and this results in fold curves of different periods on the $\epsilon = 0$ axis being very close together (as seen in Figure 5). This leads to an overlap of fold curves of many different periods and to multiple solution behaviour being possible, as shown for two values of a in Figure 7. Furthermore, in all cases the effect of increasing ϵ (the strength of the seasonal forcing) is substantial when the parameter choice gives rise to both a stable equilibrium and stable limit cycles in the unforced system.

Whilst there are many similarities in the bifurcation diagrams for the different values of a, variation in the initial period of the unforced system has important consequences for the different dynamics possible in the forced system, specifically the range of stable periodic solutions. Lower period cycles are only possible for the larger values of a tested. Apart from this difference in period, the bifurcation diagrams change more generally, as seen in Figure 6, where the Neimark-Sacker bifurcation curve for the yearly cycles (NS1) moves up in δ as a increases. In the $a = 5$ case, the Neimark-Sacker curve also becomes less horizontal so that it is possible to move from a stable equilibrium to quasi-periodicity and chaos by increasing ϵ and keeping all other parameters constant. The fold regions are also much wider for $a = 5$ indicating that seasonal forcing has an effect for a wider range of δ values in this case. From Figures 5 and 6, it is clear that there is a considerable difference in the dynamics between low values of a, say $a = 1.5$ or 1.7 which are in the range given for the red grouse system, compared to $a = 5$, with the inference that seasonal forcing has more of an impact for the higher values of a tested.

The largest fold and stability regions for $a = 4$ and $a = 5$ are much larger than those for lower values of a (as seen in Figure 5). This raises an interesting question: is this occurring because lower period cycles resonate more, creating more stability for the multi-year cycles of lower period, in comparison to those of higher period? This could be because the 3 and 4 year cycles are closer in period to the forcing (1 year). Or are the regions larger because the initial amplitude of the limit cycles in the unforced system is higher, causing more resonance when forcing is introduced? Or is it the fact that a is now much larger: since a is the parameter being annually forced this could lead to greater resonance and hence larger fold regions? One approach to gain some insight into this would be to produce a similar figure to Figure 5 with the same range of a values, but with a different parameter being seasonally forced. This is a natural area for future study.

4 Discussion

Seasonal forcing has been well studied in both interacting population and microparasite systems (Choisy et al., 2006; Greenman et al., 2004; Kuznetsov and Piccardi, 1994; Rinaldi et al., 1993). As in this host-macroparasite study, these have all shown that seasonal forcing can lead to multi-year cycles, quasi-periodicity, chaos and multiple solution behaviour. Other similarities include the increased amplitude in population abundance of the multi-year cycle solutions compared to the yearly cycle and the significant impact on the dynamics observed through increasing the amplitude of forcing. The similarities are particularly true for systems in which there is a Hopf bifurcation present in the unforced dynamics, since this is the determining factor for the existence of quasi-periodicity and is influential in the production of the fold curves (although these can occur when non-cyclic systems are forced (Kuznetsov and Piccardi, 1994; Taylor et al., 2013a)).

However, seasonal forcing within this host-macroparasite systems shows some important differences to ecological and microparasite systems. One of the most noticeable aspects of this host-macroparasite system is the existence of a wide range of different period solutions, with sizable regions of stability for 3 to 16 year cycles as well as an 18 year cycle found by simulation and the numerous period-doubling bifurcations to higher period cycles. This indicates that host-macroparasite interactions, including the red grouse system, are able to experience many different periodic solutions. In contrast, data for predator-prey systems often show a smaller range of cycles such as 3-5 years for Fennoscandian voles (Bjørnstad et al., 1995) or 8-11 years for the snowshoe hare and lynx cycles (Murray, 2000). Also, in the measles literature, cycles of 1-3 years are most common, although there is the possibility of cycles with periods of up to 8 years (Earn et al., 2000). In the host-macroparasite system the wide range of cyclic dynamics occurs due to the rapid increase of the limit cycle period from the Hopf bifurcation in the unforced system.[1] Thus the bifurcation diagram shows that the fold curves overlap to a much greater extent than is typical for interacting population and microparasite systems (Kuznetsov and Piccardi, 1994; Rinaldi et al., 1993). Not only does this rapid increase in the unforced period lead to the wide range of different period cycles but most importantly, it leads to an increased chance of multiple solution behaviour. While multiple solutions do occur in interacting population and microparasite systems, it is often for a small number of parameter sets and is usually restricted to 2 or 3 different solution possibilities (Earn et al., 2000; Taylor et al., 2013b). In contrast, Figure 6 shows that multiple solution behaviour is possible for a wide range of δ

[1] Comparison of rapidity of the increase is based upon observing the relative width of the fold curves in comparison to the distance between the cusp of each fold curve on the axis.

and ϵ values for all values of a tested, and in Figure 7 the points tested have at least 5 different solutions possible. Furthermore, the wide range of periodic dynamics and the multiple solution behaviour combine so that both higher and lower period cycles can be found in the resulting dynamics for the same parameter values. For example, in Figure 7(c) both 4 and 18 year cycles occur in simulations for the same parameter values but different initial conditions.

There are other aspects of the bifurcation diagrams shown here for host-macroparasite systems which differ from seasonal models of interacting population and microparasite systems. The Neimark-Sacker bifurcation curves are, generally, almost horizontal (Figure 6) which is not usually the case for interacting population and microparasite systems (Kuznetsov and Piccardi, 1994; Rinaldi et al., 1993), and indicates that the unforced dynamics are a good predictor of the split between yearly cycles and quasi-periodic dynamics. Also, our results indicate several regions of (apparently) chaotic behaviour, due to the many period-doubling bifurcation curves which can give rise to period-doubling cascades (Aron and Schwartz, 1984). This multitude of period-doubling cascades is not readily observed in other seasonal systems (O'Regan et al., 2013; Rinaldi et al., 1993). Our study also shows that period-halving can occur, which has not been reported in previous studies of seasonally forced models. This highlights the importance of the period-doubling bifurcations on the resultant population dynamics.

Small perturbations in the strength of the seasonal forcing or other parameters can lead to significantly different dynamics through a change of period and amplitude, or to quasi-periodic or chaotic solutions. This is in contrast to the unforced model, where a small change in parameter values would lead to a relatively small change in the period of the limit cycles (unless the parameters are very close to the Hopf bifurcation, in which case switches between a stable equilibrium and limit cycles could occur). In Figure 10, a simulation showed the effect of a perturbation in the host population abundance (but no change of any parameters), which led to a change in cycle period and amplitude. This sensitivity to perturbations leads to difficulties in determining the factors that are the key drivers of population cycles and in explaining the causes of shifts in population behaviour. Furthermore, since multiple solutions can exist for a single parameter set it is not possible at the outset to predict the resulting population dynamics.

The literature on red grouse documents a very wide range of periods of population cycles in England and Scotland, with reported periods varying between 4-8 years (Hudson et al., 1998), 3-13 years (Cattadori et al., 2005b) or 2-15 years (Haydon et al., 2002). The driver of red grouse cycles is subject to debate, with infection from the nematode macroparasites and territorial behaviour seen as the most likely causative factors (Dobson and Hudson, 1992; Hudson et al., 1998; Redpath et al., 2006). It has also been shown that there is no strong latitudinal variation

in periodicity but rather a plethora of intermixing periods across the whole of England and Scotland (Haydon et al., 2002). Both these aspects are consistent with our results. With parameter values corresponding to red grouse populations across England and Scotland, the host-macroparasite model showed a wide range of periodic cycles and multiple solution behaviour were found (Figures 5, 7). In the model it is possible for two geographically close populations of red grouse to have very similar life-history parameters and yet show exceedingly different dynamics such as low period and high period cycles with different amplitudes. Furthermore, the sensitivity to perturbations may explain the difficulty in determining cyclicity and the presence of only weakly cyclic time-series data (Haydon et al., 2002). This suggests that seasonal forcing may be an important factor in producing the wide range of cyclic periods observed in red grouse population dynamics and can have a significant impact on the dynamics of host-macroparasite system in general.

Appendix A Model Details

To aid readers unfamiliar with mathematical models of host-macroparasite systems, a full description of the derivation of (2.1) is provided here. The number of parasites within each host are modelled explicitly producing an infinite set of equations. Let $p_i(t)$ be the number of hosts which are infected with i parasites at time t (hence $p_0(t)$ are hosts which have no parasites at time t). This leads to $\sum_{i=0}^{\infty} p_i$ equalling total host population and $\sum_{i=0}^{\infty} ip_i$ the total macroparasite population. We include birth and death of hosts, transmission and death of parasites and explicitly model the free-living larval stage of the parasites, $L(t)$, the total number of larvae at time t. This produces the following model equations:

$$\begin{aligned}
\frac{dp_0}{dt} =& a^* \sum_{i=0}^{\infty} p_i - \delta^* \sum_{i=0}^{\infty} ip_i - bp_0 - \beta^* Lp_0 + \mu^* p_1 \\
\frac{dp_i}{dt} =& -bp_i - \alpha ip_i - \mu^* ip_i + \mu^*(i+1)p_{i+1} - \beta^* Lp_i + \beta^* Lp_{i-1} \quad \text{for } i = 1 \ldots \infty \\
\frac{dL}{dt} =& \lambda \sum_{i=0}^{\infty} ip_i - \gamma^* L - \beta^* L \sum_{i=0}^{\infty} p_i.
\end{aligned} \tag{A.1}$$

The first two equations show how the populations of hosts with no parasites and i parasites change with time. a is the birth rate of hosts; any host can give birth but all new hosts are free from parasites hence all births arrive into this first class. δ is the reduction in fecundity caused by the parasite, which decreases the birth of new hosts in proportion to the number of parasites within each host. This term can cause the birth rate to become negative when there are large numbers of parasites, which is clearly unrealistic. Nevertheless, the linear relationship is suggested by field experiments. Several authors have used nonlinear terms to prevent the

possibility of a negative birth rate (Diekmann and Kretzschmar, 1991; Rosà and Pugliese, 2002), but they do not find significant differences in results for realistic parameter values. Therefore we retain the original formulation of May and Anderson (1978), which is also used in other models (Dobson and Hudson, 1992; White et al., 1996). The rate of natural host death is given by b; we assume that death of a host leads to death of the parasites within that host. A host becomes infected by a macroparasite through contact with larvae L, with transmission rate β. In the second equation, this leads to gains into the p_i class through a host with $i-1$ parasites becoming infected by another parasite and similarly, losses are caused by a host with i parasites gaining a new parasite and moving into the p_{i+1} class. μ is the natural death rate of parasites within hosts, consequently leading to hosts moving from having i parasites to having $i-1$ parasites, where any of those i parasites can die. This leads to the two terms involving μ in the second equation. Death of hosts caused by the parasites occurs at rate αi i.e. it is proportional to the number of parasites within the host. Lastly, in the larvae equation all the parasites are able to produce larvae at rate λ and the larvae have natural death rate of γ. The larvae come into contact with hosts and have successful transmission at rate β. We assume that once a larvae enters a host it becomes a mature parasite.

We now let $H = \sum_{i=0}^{\infty} p_i$ and $P = \sum_{i=0}^{\infty} i p_i$. Hence the following hold true:

$$\begin{aligned} \frac{dH}{dt} &= \frac{dp_0}{dt} + \sum_{i=1}^{\infty} \frac{dp_i}{dt} \\ \frac{dP}{dt} &= 0.\frac{dp_0}{dt} + \sum_{i=1}^{\infty} i.\frac{dp_i}{dt}. \end{aligned} \tag{A.2}$$

When performing these calculations many terms cancel each other out, which leads to the following equations:

$$\begin{aligned} \frac{dH}{d\tau} &= (a^* - b)H - (\alpha + \delta^*)P \\ \frac{dP}{d\tau} &= \beta^* LH - (\mu^* + b)P - \alpha \sum_{i=0}^{\infty} i^2 p_i \\ \frac{dL}{d\tau} &= \lambda P - \gamma^* L - \beta^* LH. \end{aligned} \tag{A.3}$$

The last term in the second equation arises because the number of parasites within a host affects the likelihood of a host dying due to parasitism. Thus, it is necessary to know how the parasites are spread throughout the host population. To do this, we first change variable by letting $\tilde{p}_i = \frac{p_i}{H}$ and interpret $\tilde{p}_i$ as the probability that a host has i parasites. This leads to the following change in (A.3):

$$\alpha \sum_{i=0}^{\infty} i^2 p_i = \alpha H \sum_{i=0}^{\infty} i^2 \tilde{p}_i. \tag{A.4}$$

The negative binomial distribution is commonly assumed for the distribution of $\tilde{p}_i$ (Anderson and May, 1978; Diekmann and Kretzschmar, 1991; Rosà and Pugliese, 2002), as it represents

the fact that a minority of hosts harbour the majority of parasites. The negative binomial can be described using two parameters, m and k, where m is the mean number of parasites per host, i.e. $m = \frac{P}{H}$ and k is the aggregation parameter. The parasites become more evenly spread amongst hosts as k increases. Thus, the negative binomial assumption leads to:

$$\sum_{i=0}^{\infty} i^2 \tilde{p}_i = \frac{P}{H} + \left(\frac{P}{H}\right)^2 \frac{k+1}{k}, \tag{A.5}$$

which produces the form of (2.1) when substituted into (A.3).

References

S. Altizer, A. Dobson, P. Hosseini, P. Hudson, M. Pascual, and P. Rohani. Seasonality and the Dynamics of Infectious Diseases. *Ecol. Lett.*, 9:467–484, 2006. doi: 10.1111/j.1461-0248.2005.00879.x.

R. Anderson. *Nematode parasites of vertebrates: their development and transmission.* Cabi Wallingford, UK, 2000.

R. Anderson and R. May. Regulation and stability of host-parasite population interactions: I. regulatory processes. *J. Anim. Ecol.*, pages 219–247, 1978. doi: 10.2307/3933.

R. Anderson and R. May. *Infectious diseases of humans: dynamics and control*, volume 28. Oxford University Press Oxford, UK, 1992.

J. Aron and I. Schwartz. Seasonality and period-doubling bifurcations in an epidemic model. *J. Theor. Biol.*, 110 (4):665–679, 1984. doi: 10.1016/S0022-5193(84)80150-2.

O. Bjørnstad, W. Falck, and N. Stenseth. A Geographic Gradient in Small Rodent Density Fluctuations: A Statistical Modelling Approach. *Proc. R. Soc. B*, 262:127–133, 1995. doi: 10.1098/rspb.1995.0186.

L. Bolzoni, A. Dobson, M. Gatto, and G. De Leo. Allometric Scaling and Seasonality in the Epidemics of Wildlife Diseases. *Am. Nat.*, 172:818–828, 2008. doi: 10.1086/593000.

I. Cattadori, B. Boag, O. Bjørnstad, S. Cornell, and P. Hudson. Peak shift and epidemiology in a seasonal host–nematode system. *Proc. R. Soc. B*, 272(1568):1163–1169, 2005a. doi: 10.1098/rspb.2004.3050.

I. Cattadori, D. Haydon, and P. Hudson. Parasites and climate synchronize red grouse populations. *Nature*, 433 (7027):737–741, 2005b. doi: 10.1038/nature03276.

M. Choisy, J. Guegan, and P. Rohani. Dynamics of Infectious Diseases and Pulse Vaccination: Teasing Apart the Embedded Resonance Effects. *Phys. D*, 223:26–35, 2006. doi: 10.1016/j.physd.2006.08.006.

S. Cornell, O. Bjørnstad, I. Cattadori, B. Boag, and P. Hudson. Seasonality, cohort-dependence and the development of immunity in a natural host–nematode system. *Proc. R. Soc. B*, 275(1634):511–518, 2008. doi: 10.1098/rspb.2007.1415.

T. Coulson, E. Catchpole, S. Albon, B. Morgan, J. Pemberton, T. Clutton-Brock, M. Crawley, and B. Grenfell. Age, sex, density, winter weather, and population crashes in soay sheep. *Science*, 292(5521):1528–1531, 2001. doi: 10.1126/science.292.5521.1528.

O. Diekmann and M. Kretzschmar. Patterns in the effects of infectious diseases on population growth. *J. Math. Biol.*, 29(6):539–570, 1991. doi: 10.1007/BF00164051.

K. Dietz. *The Incidence of Infectious Disease Under the Influence of Seasonal Fluctuations*, volume 11 of *Lecture Notes in Biomathematics: Mathematical Models in Medicine*, pages 1–15. Springer-Verlag, Berlin, Germany, 1976. doi: 10.1007/978-3-642-93048-5_1.

A. Dobson and P. Hudson. Regulation and stability of a free-living host-parasite system: Trichostrongylus tenuis in red grouse. ii. population models. *J. Anim. Ecol.*, pages 487–498, 1992. doi: 10.2307/5339.

E. Doedel. AUTO, A Program for the Automatic Bifurcation Analysis of Autonomous Systems. *Congr. Numer.*, 30:265–384, 1981.

F. Doveri, M. Scheffer, S. Rinaldi, S. Muratori, and Y. Kuznetsov. Seasonality and Chaos in a Plankton-Fish Model. *Theor. Popul. Biol.*, 43:159–183, 1993. doi: 10.1006/tpbi.1993.1008.

J. Dushoff, J. Plotkin, S. Levin, and D. Earn. Dynamical Resonance Can Account for Seasonality of Influenza Epidemics. *Proc. Natl. Acad. Sci. USA*, 101:16915–16916, 2004. doi: 10.1073/pnas.0407293101.

D. Earn, P. Rohani, B. Bolker, and B. Grenfell. A Simple Model for Complex Dynamical Transitions in Epidemics. *Science*, 287:667–670, 2000. doi: 10.1126/science.287.5453.667.

B. Finkenstadt and B. Grenfell. Time Series Modelling of Childhood Diseases: A Dynamical Systems Approach. *J. R. Stat. Soc. Ser. C. Appl. Stat.*, 49:187–205, 2000. doi: 10.1111/1467-9876.00187.

J. Greenman, M. Kamo, and M. Boots. External Forcing of Ecological and Epidemiological Systems: A Resonance Approach. *Phys. D*, 190:135–151, 2004. doi: 10.1016/j.physd.2003.08.008.

F. Gulland. The role of nematode parasites in soay sheep (ovis aries l.) mortality during a population crash. *Parasitology*, 105:493–493, 1992. doi: 10.1017/S0031182000074679.

F. Gulland. *Ecology of infectious diseases in natural populations*, chapter The impact of infectious diseases on wild animal populations-a review, pages 20–51. Cambridge University Press, Cambridge, 1995. doi: 10.1017/CBO9780511629396.002.

F. Gulland and M. Fox. Epidemiology of nematode infections of soay sheep (ovis aries l.) on st kilda. *Parasitology*, 105:481–481, 1992. doi: 10.1017/S0031182000074667.

D. Haydon, D. Shaw, I. Cattadori, P. Hudson, and S. Thirgood. Analysing noisy time–series: describing regional variation in the cyclic dynamics of red grouse. *Proc. R. Soc. B*, 269(1500):1609–1617, 2002. doi: 10.1098/rspb.2002.2053.

P. Hudson, D. Newborn, and A. Dobson. Regulation and stability of a free-living host-parasite system: Trichostrongylus tenuis in red grouse. i. monitoring and parasite reduction experiments. *J. Anim. Ecol.*, pages 477–486, 1992. doi: 10.2307/5338.

P. Hudson, A. Dobson, and D. Newborn. Prevention of population cycles by parasite removal. *Science*, 282(5397): 2256–2258, 1998. doi: 10.1126/science.282.5397.2256.

E. Korpimaki and C. Krebs. Predation and Population Cycles of Small Mammals: A Reassessment of the Predation Hypothesis. *Bioscience*, 46:754–764, 1996.

Y. Kuznetsov. *Elements of Applied Bifurcation Theory*. Springer-Verlag, New York, NY, 1995.

Y. Kuznetsov and C. Piccardi. Bifurcation Analysis of Periodic SEIR and SIR Epidemic Models. *J. Math. Biol.*, 32:109–121, 1994. doi: 10.1007/BF00163027.

R. May and R. Anderson. Regulation and stability of host-parasite population interactions: II. destabilizing processes. *J. Anim. Ecol.*, pages 249–267, 1978. doi: 10.2307/3934.

D. Murray. A Geographic Analysis of Snowshoe Hare Population Demography. *Can. J. Zool.*, 78:1207 – 1217, 2000. doi: 10.1139/z00-025.

S. O'Regan, T. Kelly, A. Korobeinikov, M. O'Callaghan, A. Pokrovskii, and D. Rachinskii. Chaos in a seasonally perturbed sir model: avian influenza in a seabird colony as a paradigm. *J. Math. Biol.*, 67(2):293–327, 2013. doi: 10.1007/s00285-012-0550-9.

S. Redpath, F. Mougeot, F. Leckie, D. Elston, and P. Hudson. Testing the role of parasites in driving the cyclic population dynamics of a gamebird. *Ecol. Lett.*, 9(4):410–418, 2006. doi: 10.1111/j.1461-0248.2006.00895.x.

S. Rinaldi, S. Muratori, and Y. Kuznetsov. Multiple Attractors, Catastrophes and Chaos in Seasonally Perturbed Predator-Prey Communities. *Bull. Math. Biol.*, 55:15–35, 1993. doi: 10.1007/BF02460293.

M. Roberts and B. Grenfell. The population dynamics of nematode infections of ruminants: periodic perturbations as a model for management. *Math. Med. Biol.*, 8(2):83–93, 1991. doi: 10.1093/imammb/8.2.83.

M. Roberts and B. Grenfell. The population dynamics of nematode infections of ruminants: The effect of seasonally in the free-living stages. *Math. Med. Biol.*, 9(1):29–41, 1992. doi: 10.1093/imammb/9.1.29.

R. Rosà and A. Pugliese. Aggregation, stability, and oscillations in different models for host-macroparasite interactions. *Theor. Popul. Biol.*, 61(3):319–334, 2002. doi: 10.1006/tpbi.2002.1575.

J. Sherratt and M. Smith. Periodic travelling waves in cyclic populations: field studies and reaction–diffusion models. *J. R. Soc. Interface*, 5(22):483–505, 2008. doi: 10.1098/rsif.2007.1327.

M. J. Smith, A. White, J. A. Sherratt, S. Telfer, M. Begon, and X. Lambin. Disease Effects on Reproduction can cause Population Cycles in Seasonal Environments. *Journal of Animal Ecology*, 77:378–389, 2008. doi: 10.1111/j.1365-2656.2007.01328.x.

R. A. Taylor, J. A. Sherratt, and A. White. Seasonal Forcing and Multi-year Cycles in Interacting Populations: Lessons from a Predator-Prey Model. *J. Math. Biol.*, 2013a. doi: 10.1007/s00285-012-0612-z.

R. A. Taylor, A. White, and J. A. Sherratt. How do Variations in Seasonality Affect Population Cycles? *Proc. R. Soc. B*, 280(1754), 2013b. doi: 10.1098/rspb.2012.2714.

P. Turchin. *Complex Population Dynamics*. Princeton University Press, Princeton, NJ, 2003.

K. White and B. Grenfell. Regulation of complex host dynamics by a macroparasite. *J. Theor. Biol.*, 186(1): 81–91, 1997. doi: 10.1006/jtbi.1996.0344.

622 K. White, B. Grenfell, R. Hendry, O. Lejeune, and J. Murray. Effect of seasonal host reproduction on host-
623 macroparasite dynamics. *Math. Biosci.*, 137(2):79–99, 1996. doi: 10.1016/S0025-5564(96)00061-2.

624 K. Wilson, O. Bjørnstad, A. Dobson, S. Merler, G. Poglayen, S. Randolph, A. Read, and A. Skorping. *The ecology*
625 *of wildlife diseases*, chapter Heterogeneities in macroparasite infections: patterns and processes, pages 6–44.
626 Oxford University Press Oxford, UK, 2002.